Preequilibrium emission and target-projectile-like correlations for $^{20}Ne+^{60}Ni$ at $E(^{20}Ne)=740$ MeV

A. D'Onofrio
Istituto Nazionale di Fisica Nucleare, 80125 Napoli, Italy, Oak Ridge National Laboratory, Oak Ridge, Tennessee 37831, and Joint Institute for Heavy Ion Research, Oak Ridge, Tennessee 37831

J. Gomez del Campo
Oak Ridge National Laboratory, Oak Ridge, Tennessee 37831

B. Delaunay, J. Delaunay, and H. Dumont
Service de Physique Nucleaire-Basse Energie, Centre d'Etudes Nucleaires de Saclay, 91191 Gif-sur-Yvette CEDEX, France

F. Andreozzi, A. Brondi, R. Moro, M. Romano, and F. Terrasi
Dipartimento di Scienze Fisiche dell'Universita, 80125 Napoli, Italy and Istituto Nazionale di Fisica Nucleare, 80125 Napoli, Italy
(Received 16 September 1988)

Inclusive γ rays at 90° and 125° and particle spectra (for $Z=1$ to 6) at 14° and ($Z=1$ to 4) at 120° and 150° were measured. Particle-γ-ray coincidences were obtained. Cross sections for heavy residuals were extracted from in-beam γ-ray and radioactivity measurements. Target-projectile-like correlations were well reproduced using a geometrical abrasion model plus preequilibrium and equilibrium decay.

I. INTRODUCTION

The study of reaction mechanisms in the intermediate energy domain of 10–100 MeV/nucleon, is a subject of growing interest. The transition between the low-energy regime, where a description of the interactions in terms of the mean field seems appropriate,[1] to the relativistic region where a geometric description of the interactions between two sets of free nucleons has been successfully applied,[2] is not yet completely understood.

A number of phenomenological descriptions to interpret the data available have been suggested. In these kinds of analysis thresholds or limiting values for physical quantities like the incident energy or the linear momentum transfer have been proposed. The speed of sound and the Fermi energy in the nucleus have been interpreted as thresholds for significant loss of the mean-field character of the interaction. On the other hand, a limiting value for the average linear momentum transfer of about 180 MeV/c has been found for central collisions in a wide range of entrance channels and incident energies.[3] The coexistence of the two extreme descriptions seems now established and great theoretical efforts are in progress to describe the interactions in a more microscopic way.[4]

For situations where one or more components of the reaction mechanism can be isolated, it is possible to gain information about the parameters relevant to the calculations. For example, in Ref. 5 a relationship between the targetlike mass distribution and the impact parameter was found, showing that an interpretation of the evolution of the reaction mechanism, from fusionlike to participant-spectator type, as a function of the "centrality" of the collisions was possible. Moreover, the observation of heavy fragments ($Z \geq 3$) emitted from equilibrated systems gave information about the mass, the angular momentum, and the excitation energy of such systems formed at high temperature.[6]

The work reported here concerns the study of the reaction $^{20}Ne+^{60}Ni$ at 740 MeV incident energy, where inclusive and exclusive measurements have been performed. Some results from the same set of data have been already published in short communications.[5,6]

II. EXPERIMENTAL ARRANGEMENT

The experiment was performed at the SARA facility in Grenoble using a 740 MeV $^{20}Ne(9+)$ beam, with an average intensity of 40 nA. Isotopically enriched self-supporting targets of ^{60}Ni, 1 mg/cm^2 and 5 mg/cm^2 thick were used. A cylindrical scattering chamber of 500 mm diameter and 160 mm height was utilized. Two openings, one on the bottom, and the other on the side of the chamber at 125° with respect to the beam direction, allowed the positioning of two γ-X Ge detectors. The first detector was 150 mm away from the target, and the second 170 mm; two conic-shaped lead diaphragms 50 mm thick, were used to define the solid angles of 51 msr and 43 msr, respectively. The efficiencies of the Ge detectors were 21% and their energy resolution about 1.9 keV for the 1.33 MeV line of ^{60}Co. A large asymmetric NaI anti-Compton shield surrounded the Ge detector

placed at the bottom of the scattering chamber. Charged particles were detected using three particle telescopes. Two of them were solid-state telescopes consisting of three silicon detectors with thicknesses of 23 μm, 75 μm, and 5 mm and 13 μm, 53 μm, and 5 mm positioned at 120° and 150° with respect to the beam direction, respectively. The third telescope, placed at 14°, consisted of two silicon detectors (48 μm and 1000 μm) followed by a 10 cm thick NaI crystal. The solid angles (in msr) subtended by the charged-particle detectors placed at 14°, 120°, and 150° were 1.39, 11, and 13, respectively.

The following kind of data were acquired: coincidence events between the γ rays detected by the Ge at 90° and the charged particle detected at 14°, 120°, or 150°; coincidences between the charged particles at 14° and those detected at 120° or 150°; singles γ-ray and charged-particle energy spectra. Data were stored event by event on magnetic tapes for further analysis. The collected charge was measured in a Faraday cup located 6 m downstream from the target. Energy calibrations of the Si detectors were achieved using an alpha source of ^{222}Rn and a pulse generator. The energy calibration of the NaI element of the counter telescope used at 14° was achieved by identifying the particle in mass and charge with the usual pulse height vs ΔE (solid-state) plot. Once the mass and charge are known the energy deposited in the NaI can be inferred from the measured stopping powers of the two ΔE elements.

III. EXPERIMENTAL RESULTS

A. Singles data

The singles in-beam and radioactivity gamma-ray measurements were used to extract the absolute cross sections for several residual nuclei identified by their characteristic gamma lines. These results have been discussed in more detail in Ref. 5.

The singles energy spectra for charged particles of $Z=2$ and 3 detected at 14°, are shown in Fig. 1 and those for 120° and 150° are shown in Fig. 2. The dashed and solid lines correspond to theoretical predictions discussed below and in Sec. V. The spectra obtained at 14° present two components: one at high energy about 70% of the beam velocity and the other at a low energy which approximately corresponds to the Coulomb separation of the particle from the composite system. In contrast, in the 120° and 150° spectra only one component at low energy and with Maxwellian-type shape typical of evaporative phenomena can be seen. The energy spectra $(d^2\sigma/d\Omega dE)$ at these backward angles were fitted using a moving source model with the following formula:

$$(d^2\sigma/d\Omega dE)=C(B_c,E)\exp(-E/T)/(\sin^n\theta)\ , \qquad (1)$$

where E is the particle kinetic energy expressed in the rest frame of the source, T is the usual slope (effective temperature) parameter, and n is a number that reflects the degree of anisotropy of the angular distribution of the emitted particle with respect to the source. The kinetic energy E can be expressed in terms of the source speed V_s, particle laboratory energy $E_{\rm lab}$, and the emission angle $\theta_{\rm lab}$ by

$$E=E_s+E_{\rm lab}-2(E_sE_{\rm lab})^{1/2}\cos\theta_{\rm lab}\ , \qquad (2)$$

where $E_s=1/2\,A_pV_s^2$ and A_p is the projectile mass number. The term $C(B_c,E)$ is an effective transmission coefficient given by

$$C(B_c,E)=\{1+\exp[(B_c-E)/\Delta B_c]\}^{-1}\ , \qquad (3)$$

where B_c, the Coulomb barrier, is given by $B_c=1.44ZpZ_s-Z_p)/R_{12}$, with $R_{12}=1.55[A_p^{1/3}+(A_s-A_p)^{1/3}]$ and $\Delta B_c=0.1B_c$. The mass A_s and speed V_s of the source, for the present analysis, are average values derived using the abrasion-ablation model discussed in Sec. V.

The results of the fits to the spectra at 120° and 150° us-

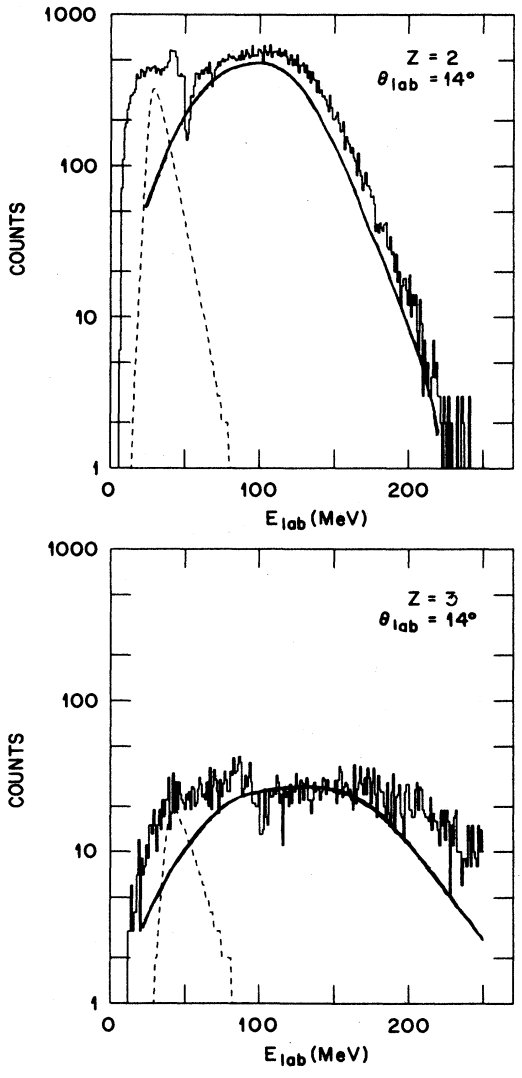

FIG. 1. Forward angle energy spectra for ^{20}Ne+^{60}Ni at $E_{\rm lab}=740$ MeV. The dashed lines are the results of a calculation using Eq. (1) and the parameters of Table I. The solid curves are the result of the abrasion-preequilibrium-ablation calculation discussed in the text.

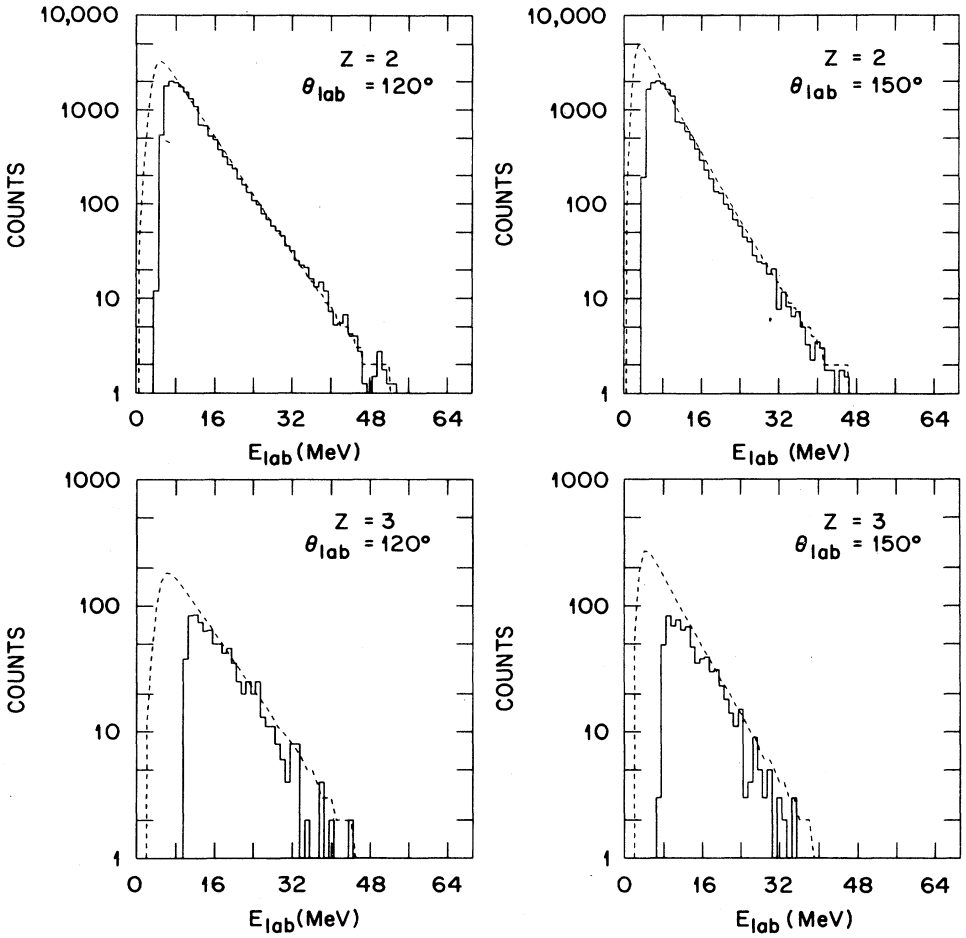

FIG. 2. Backward-angle energy spectra for $^{20}Ne+^{60}Ni$ at $E_{lab}=740$ MeV. The dashed curves represent the results of best fits to the experimental spectra at 120° and 150° using Eq. (1).

ing (1) are shown by the dashed lines of Figs. 1 and 2, where the T and n parameters, resulting from the best fit, are given in Table I. The extracted V_s values are about $0.05c$ or 40% less than the full momentum transfer value. These V_s values are consistent with the incomplete momentum transfer systematics[3] and with the abrasion-ablation calculations discussed in Sec. V. In Table I one can observe that the slope parameter T for the $Z=1$ fragments increases with mass and is larger for ^{3}He and Li isotopes than for ^{4}He. Also the p and d angular distributions are consistent with an isotropic emission ($n=0$) while those from t to Li show an anisotropy increasing with mass of the emitted particle. Neglecting the uncertainties in the V_s and A_s of the source, these findings can be interpreted in the framework of the statistical model. In particular, the higher slope parameters (T) seen for d, t, ^{3}He, and Li (see Table I) compared to p and α are generally consistent with cluster emissions which occur mostly in the first stages of the deexcitation process, whereas the p and α emission are important during all the deexcitation stages. The behavior of the angular distribution parameters (n) is equally consistent with angular momentum effects in the statistical emission process. In fact, the p and d emission involves small orbital angular momentum ($l\approx 0$) which in turn produces isotropic angular distributions, whereas the heavier-mass particles carry away more angular momentum and are emitted from states in the source of higher total angular momentum, thus producing more aligned (closer to $n=1$) angular distributions. The solid lines shown in Fig. 1, as well as more features of the statistical emission process will be discussed in Sec. V.

TABLE I. Parameters of moving source analysis using Eq. (1). See text for explanation of symbols.

Particle	E_s (MeV)	B_c (MeV)	T (MeV)	n
p	1.4	5.6	4	0
d	2.08	5.4	5.8	0
t	2.78	5.2	6.6	0.2
^{3}He	2.78	10.0	7.8	0.2
^{4}He	3.7	10.2	5.6	0.6
Li	6.0	14.0	8.0	0.6

B. Coincidence data

The first set of coincidence data that will be discussed concerns the coincidences between the high-energy component of the spectra at 14° (see Fig. 1) for $Z=2$ to 6, and the target-like residues detected via their discrete γ lines. The analysis of the correlation between target-like residues of mass A and the emitted fragments at 14° of charge Z can be performed by defining the quantity F,

$$F=Y_c(A,Z)/[Ys(A)Y_s(Z)]\,, \tag{4}$$

where $Y_c(A,Z)$ is the coincidence yield between A and Z, and $Y_s(A)$ and $Y_s(Z)$ are the singles yields of product A and ejectile Z, respectively. The results of the correlation function F for ejectiles from $Z=2$ to $Z=6$ are given in Fig. 3. It should be noticed that no correlations were seen between light ejectiles and target recoils above $A=58$, and as can be seen from the figure all correlations show considerable strength for masses far below the target ($A=60$). This observation indicates that there is a large energy deposition in the target, in spite of the high kinetic energy of the ejectiles.

Another set of coincidences was obtained for the backward-angle particle detectors placed at 120° and 150° and the γ rays at 90°. The major results of these coincidences concern the population of excited states for ^{7}Li and ^{7}Be. The experimental details and analysis were given in Ref. 6.

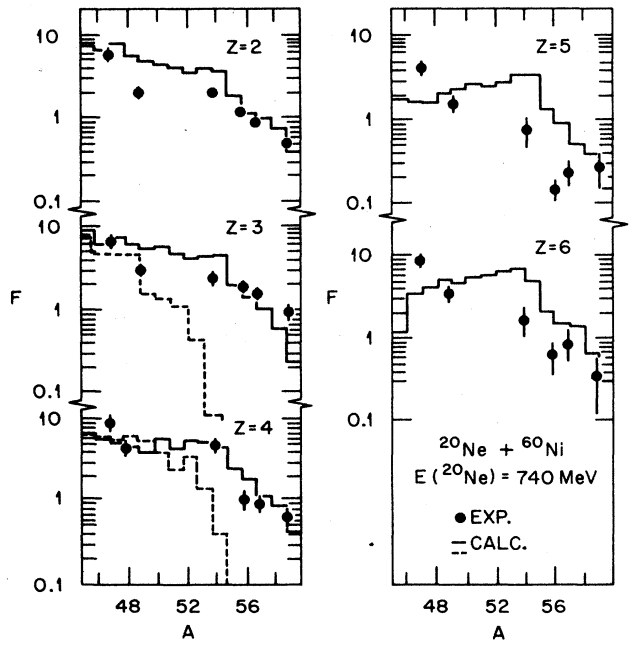

FIG. 3. Correlation functions, Eq. (4), between targetlike residues of mass A and the emitted fragments at 14° of charge Z. The solid histograms are the results of the abrasion-preequilibrium-ablation calculation discussed in the text. The dashed histograms show the influence of omitting the preequilibrium stage in the calculations.

IV. ANALYSIS OF RESULTS

In order to explain the data presented in Secs. II and III, we first need a prediction of the primary distribution. Aside from the complete fusion cross section, which in this case is expected to be very small ($\sim 10\%$ of the total reaction cross section), fragmentation of the entrance channel will be dominant.

A geometrical model (5), based on a modification of the abrasion-ablation model,[7] was chosen. As will be discussed in the next section, the model predicts a participant spectator mechanism, with the formation of a highly excited system in the nuclear overlap region, for the most peripheral interactions. For smaller impact parameters the formation of a composite system by means of a massive transfer process is predicted. Due to the high excitation energy deposited on the heavy primary fragments, preequilibrium emission has to be included. For this stage the code RELAX by M. Blann[8] was used. Finally, particle evaporation was calculated using the Monte Carlo Hauser-Feshbach code LILITA.[9]

V. ABRASION MODEL AND PREEQUILIBRIUM CALCULATIONS

The approach consists in a modified abrasion model in which the effects of Coulomb barriers and of energy dissipation in the colliding nuclei are taken into account. The reaction mechanism evolves from an intermediate rapidity source (IRS) formation for more peripheral collisions to increasingly massive transfers for lower values of the impact parameters, where IRS formation is no more energetically allowed.

One- and two-body energy dissipation are evaluated through the approximate analytical expressions obtained in Ref. 10 in the framework of a Fermi gas description of the colliding nuclei. The resulting expressions for the energy loss depend only on the distance of the closest approach d, which is deduced from the particle trajectory. The trajectory was computed using a point particle plus charged sphere Coulomb potential, and also depends on the energy dissipation. Thus a self-consistent technique was applied to arrive at the final d values. Once d is known, the number of abraded nucleons (resulting from the geometrical overlap of two spheres of uniform mass density) is determined and also the center-of-mass scattering angle and Q values. These calculations produce two-body final states targetlike (TLF) and projectilelike (PLF) or three-body states TLF, PLF, and IRS. The formation of IRS is only possible if the difference between the Q value and the dissipated energy is at least equal to the binding energy of the participant nucleons. Finally, the excitation energies of PLF and TLF are estimated from the one-body energy dissipation in each nucleus, scaled by the ratio of the abraded to the spectator volumes.

The primary fragment distribution thus obtained is shown in Table II, where the values of mass, excitation energy, and angular momentum are given. For each massive transfer an angular momentum window $[l_i(\min), l_i(\max)]$ in the entrance channel is obtained.

TABLE II. Primary distribution deduced from the Abrasion model.

b[a] (fm)	l_i(min)[b] (h)	l_i(max)[b] (k)	A_t[c]	E_t[d] (MeV)	l_t(min)[b] (h)	l_t(max)[b] (h)	l_{cr}[b] (h)	l_d[b] (h)	A_p[e]	E_p[f] (MeV)	σ[g] (mb)
3.14	0	63	80	557	0	63	55	74	0	0	191
3.44	64	69	76	552	51	55	48	67	4	37	64.5
3.71	70	74	75	509	52	55	48	67	5	36	62.3
3.98	75	80	74	483	52	56	45	67	6	35	64.8
4.23	81	85	73	460	53	55	45	67	7	34	67.6
4.49	86	90	72	423	52	54	43	67	8	33	70.0
4.74	91	95	71	397	50	52	43	65	9	31	74.0
4.99	96	100	70	359	48	50	43	65	10	29	79.2
5.24	101	105	69	333	45	47	41	64	11	27	84.5
5.50	106	110	68	308	42	44	38	64	12	24	90.5
5.76	111	115	67	257	39	40	36	63	13	21	98.0
6.04	116	121	66	232	35	36	34	63	14	18	108
6.34[h]	122	127	55	12.2	13	15		53	15	6	120
6.65[h]	128	133	56	9.9	11	13		54	16	5	136
7.00[h]	134	140	57	7.4	9	11		56	17	4	161
7.39[h]	141	148	58	5.6	7	9		57	18	3	201
7.88[h]	149	158	59	3.4	5	7		59	19	2	291

[a]Impact parameter.
[b]See text.
[c]Mass of primary targetlike fragment.
[d]Excitation energy of primary targetlike fragment.
[e]Mass of primary projectilelike fragment.
[f]Excitation energy of primary projectilelike fragment.
[g]Primary cross section.
[h]For these values of impact parameter a three-body regime is active (see text for details).

The discontinuity at $b=6.34$ is due to the fact that for this value of impact parameter the change from the massive transfer regime to the three-body regime occurs. The angular momenta l_t transferred to the composite systems were calculated using the following scaling formula:

$$l_t=(A_{\rm tr}/A_p)l_i(b)\ , \tag{5}$$

where $A_{\rm tr}$ refers to the transferred mass and $l_i(b)$ to the orbital angular momentum in the entrance channel corresponding to the impact parameter b.

In Table II the values of the angular momentum corresponding to the liquid drop (l_d) and complete fusion ($l_{\rm cr}$) limits for the different intermediate systems taken from Ref. 12 are also reported (no $l_{\rm cr}$ is reported for $b>6.04$ fm, where the three-body regime starts). As one can see most of the angular momentum windows of the massive transfer process lie systematically higher than $l_{\rm cr}$, but still below l_d. Such a situation could imply that the intermediate systems cannot evolve towards statistical equilibrium without losing angular momentum and excitation

TABLE III. Preequilibrium emission results and final angular momentum windows.

A_t[a]	E_t[a] (MeV)	N_p[b]	N_n[b]	$E_{\rm rem}$[b] (MeV)	$l_{\rm rem}$[b] (h)	l_t(min)[b] (h)	l_t(max)[b] (h)
80	557	3.4	3.4	175	21	0	42
76	552	2.7	2.6	125	15	36	40
75	509	2.6	2.3	125	15	37	40
74	483	2.2	2.2	100	12	40	44
73	460	2.1	1.8	100	12	41	43
72	423	1.8	1.7	100	12	40	42
71	397	1.7	1.4	75	9	41	43
70	359	1.3	1.2	75	9	39	41
69	333	1.2	0.92	50	6	39	41
68	307	0.91	0.85	50	6	36	37
67	257	0.71	0.50	50	6	33	34
66	232	0.46	0.41	25	3	32	33

[a]Same entries as Table II.
[b]See text.

energy through, e.g., preequilibrium stages. As already anticipated in Ref. 5, with these systems involving high values of excitation energies, one has to expect sizable amounts of preequilibrium particle emission. This kind of preequilibrium emission differs from particles emitted by the IRS source and refers exclusively to a highly excited system of mass A_t and excitation energy E_t (see Table II) which reaches equilibrium only after some preequilibrium nucleons are emitted. Preequilibrium emission was calculated using the code RELAX,[8] with exciton number $A_{tr}+2$. The results for each of the intermediate systems of Table II, corresponding to the massive transfer regime, are summarized in Table III, where the average number of emitted protons (N_p) and neutrons (N_n), and the average energy removed, E_{rem} are given. The average total angular momentum carried away by the emitted nucleons was then equated to the value for which the transmission coefficients of the corresponding nucleon-nucleus system falls to 0.5. The transmission coefficients were calculated with standard optical-model potential parameters. Table III contains the angular momentum windows, which result after preequilibrium emission (seventh and eighth columns). They are now below l_{cr} meaning that the system can be allowed to decay statistically by the emission of nucleons, alphas, and complex fragments with probabilities given by the Hauser-Feshbach formula.

The primary distribution defined in Tables II and III, with a spreading width for the excitation energy of 10% of the central value, was used as input for the code LILITA (Ref. 9) in order to obtain the target-like residue mass distribution, ejectile energy spectra and the correlation function F (see Figs. 2 and 3). For these last calculations the code was used with the option of writing the results of the Monte Carlo trials in an event-by-event format. Then a replay of the output data was carried out selecting the appropriate laboratory angles for the projectile-like fragments and assuming an angular distribution in the center of mass, for these fragments, of the type $d\sigma/d\Omega = \exp(-\theta/\Delta\theta)$ where a value of 10° was used for $\Delta\theta$. In Fig. 2 the results for the energy spectra for the $Z=2$ and 3 ejectiles are given by the solid lines, as can be seen they reproduce the shape of the high-energy component rather well. In Fig. 3, the results for the ratio F are given as solid histograms. As can be seen for all the ejectiles from $Z=2$ to 6 the calculations reproduce the data reasonably well and, in particular, they do not predict coincidences above $A=58$. This is an indication that the primary distribution is well modeled and that the energy released (which determines the final A distribution) is well estimated. The dotted histograms in Fig. 3 correspond to equilibrium decay of the primary reaction products, i.e., without any preequilibrium emission. As can be seen these calculations fail to reproduce the data. Finally in Fig. 4, the experimental total yields of target-like products, obtained from in-beam and radioactivity gamma-ray spectra (see Ref. 5 for details) are presented. The result

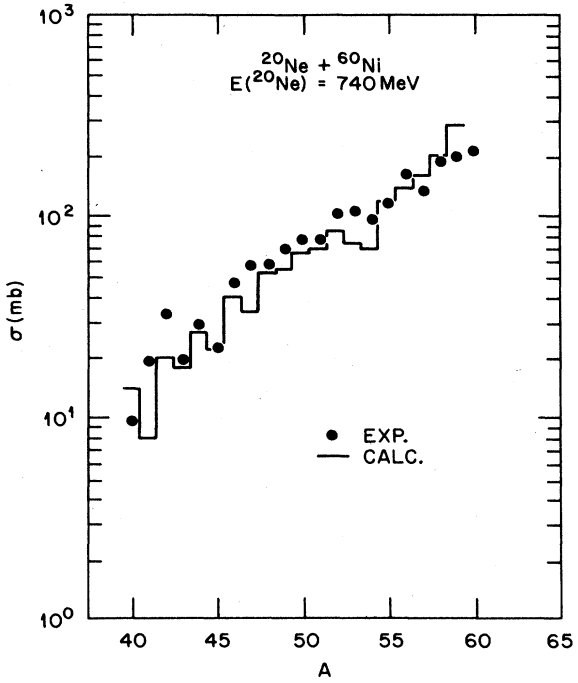

FIG. 4. Production cross section of heavy residues obtained by in-beam and radioactivity measurements. The histogram is the result of the abrasion-preequilibrium-ablation calculation discussed in the text.

of the calculation, including preequilibrium, is shown as the solid histogram and accounts very well for the data, confirming the adequacy of the primary distribution.

VI. CONCLUSIONS

Inclusive and exclusive measurements for the 740 MeV ^{20}Ne+^{60}Ni were made. A model for the primary reaction was successfully tested by comparing measurements and predictions of total cross sections for production of targetlike residuals and the correlations between these residuals and light ejectiles produced at forward angles. This model is of the geometrical abrasion-ablation type, except that the ablation stage (deexcitation) incorporates preequilibrium decay followed by the usual evaporation process. We have shown that the data suggest the formation of highly excited systems at high angular momentum. The model described in Sec. V contains an evolution of the mechanisms depending on the impact parameters involved, from fusion-like to fragmentation-type reactions. It would be very interesting to apply this model at higher bombarding energy.

Oak Ridge National Laboratory is operated by the U.S. Department of Energy under Contract No. DE-AC05-84OR21400 with Martin Marietta Energy Systems, Inc.

[1]K. T. R. Davis, K. R. S. Devi, S. E. Koonin, and M. R. Strayer, *Treatise on Heavy-Ion Science,* edited by D. A. Bromley (Plenum, New York, 1985), Vol. 3, p. 1.

[2]S. Nagamiya, J. Randrup, and T. J. M. Symons, Annu. Rev. Nucl. Part. Sci. **34**, 155 (1984).

[3]M. Conjeaud, S. Harar, M. Mostefai, E. C. Pollacco, C. Volant, Y. Cassagnou, R. Dayras, A. Legrain, H. Oeschler, and F. Saint-Laurent, Phys. Lett. **159B**, 244 (1985).

[4]H. Kruse, B. V. Jacak, J. J. Molitoris, G. D. Westfall, and H. Stocker, Phys. Rev. C **31**, 1770 (1985).

[5]A. D'Onofrio, B. Delaunay, J. Delaunay, H. Dumont, J. Goméz del Campo, F. Andreozzi, A. Brondi, R. Moro, M. Romano, F. Terrasi, and J. F. Bruandet, Phys. Rev. C **35**, 1167 (1987).

[6]A. D'Onofrio, B. Delaunay, J. Delaunay, H. Dumont, J. Gomez del Campo, A. Brondi, R. Moro, M. Romano, F. Terrasi, and J. F. Bruandet, Z. Phys. A **326**, 335 (1987).

[7]R. Dayras, A. Pagano, J. Barrette, B. Berthier, D. M. De Castro Rizzo, E. Chavez, O. Cisse, R. Legrain, M. C. Mermaz, E. C. Pollacco, H. Delagrange, W. Mittig, B. Heusch, R. Coniglione, G. Lanzano, and A. Palmeri, Nucl. Phys. **A460**, 299 (1986).

[8]M. Blann, Phys. Rev. C **31**, 1245 (1985).

[9]J. Gomez del Campo and R. G. Stokstad, Oak Ridge National Laboratory Report No. TM7295, 1981 (unpublished).

[10]S. Pal, Nucl. Phys. **A425**, 589 (1984).